frontiers | Frontiers in Environmental Science

TYPE Original Research
PUBLISHED 18 October 2022
DOI 10.3389/fenvs.2022.1040276

OPEN ACCESS

EDITED BY
Shaohua Wu,
Guangdong University of Petrochemical Technology, China

REVIEWED BY
Zimo Lou,
Zhejiang University of Technology, China
Jing Ding,
Harbin Institute of Technology, China

*CORRESPONDENCE
Zhuoyu Li,
Lizyhit@163.com

SPECIALTY SECTION
This article was submitted to Water and Wastewater Management, a section of the journal Frontiers in Environmental Science

RECEIVED 09 September 2022
ACCEPTED 05 October 2022
PUBLISHED 18 October 2022

CITATION
Wang Q, Ji Y, Hu J, Ye H, Liu Y, Wang Y, Chen C and Li Z (2022), Accelerated catalytic ozonation for aqueous nitrobenzene degradation over Ce-loaded silicas: Active sites and pathways. *Front. Environ. Sci.* 10:1040276. doi: 10.3389/fenvs.2022.1040276

Accelerated catalytic ozonation for aqueous nitrobenzene degradation over Ce-loaded silicas: Active sites and pathways

Qinghong Wang[1], Yuanyuan Ji[1], Jingze Hu[2], Huangfan Ye[1], Ya Liu[3], Yuxian Wang[1], Chunmao Chen[1] and Zhuoyu Li[1]*

[1]State Key Laboratory of Heavy Oil Processing, Beijing Key Laboratory of Oil and Gas Pollution Control, China University of Petroleum-Beijing, Beijing, China, [2]CNPC Research Institute of Safety and Environmental Technology, Beijing, China, [3]School of Chemical Engineering and Advanced Materials, The University of Adelaide, Adelaide, SA, Australia

Cerium oxides loaded silica catalysts were synthesized by an impregnation method by simply mixing Ce precursor with silica spherule (Ce/SS) and ordered MCM-41 zeolites (Ce/MCM-41), followed by a mild calcination. Compared with pure SS and MCM-41, Ce modified Ce/SS and Ce/MCM-41 demonstrate much improved catalytic ozonation activities for mineralization of recalcitrant nitrobenzene (NB). At solution pH of 6, 86 and 97% TOC mineralization rates were achieved within 60 min for Ce/MCM-41 and Ce/SS, respectively. Characterization results suggest that Ce loading significantly increases the surface Lewis acidic sites, which would synergize with Ce^{3+}/Ce^{4+} redox cycle for the activity improvement. With the aid of *in situ* electron paramagnetic resonance (EPR) spectra and quenching tests, hydroxyl radical (·OH), superoxide radical ($O_2^{\bullet-}$), and singlet oxygen ($^1O_2$) are identified as the O_3 catalytic decomposition products, while ·OH mainly accounts for NB mineralization. The detailed degradation route of NB was further investigated by the multi-chromatography analysis. NB is firstly oxidized into polyhydroxy compounds, followed by small molecular organic acids, and finally being mineralized into CO_2 and H_2O. This study established a facile strategy to synthesize highly active and stable Ce/SiO_2 catalysts for catalytic ozonation, and elucidated the in-depth mechanisms for the activity origins of the Ce loaded silica-based materials in catalytic ozonation processes (COP).

KEYWORDS

catalytic ozonation, Ce loaded silica catalysts, hydroxyl radical-based oxidation, active sites, degradation route

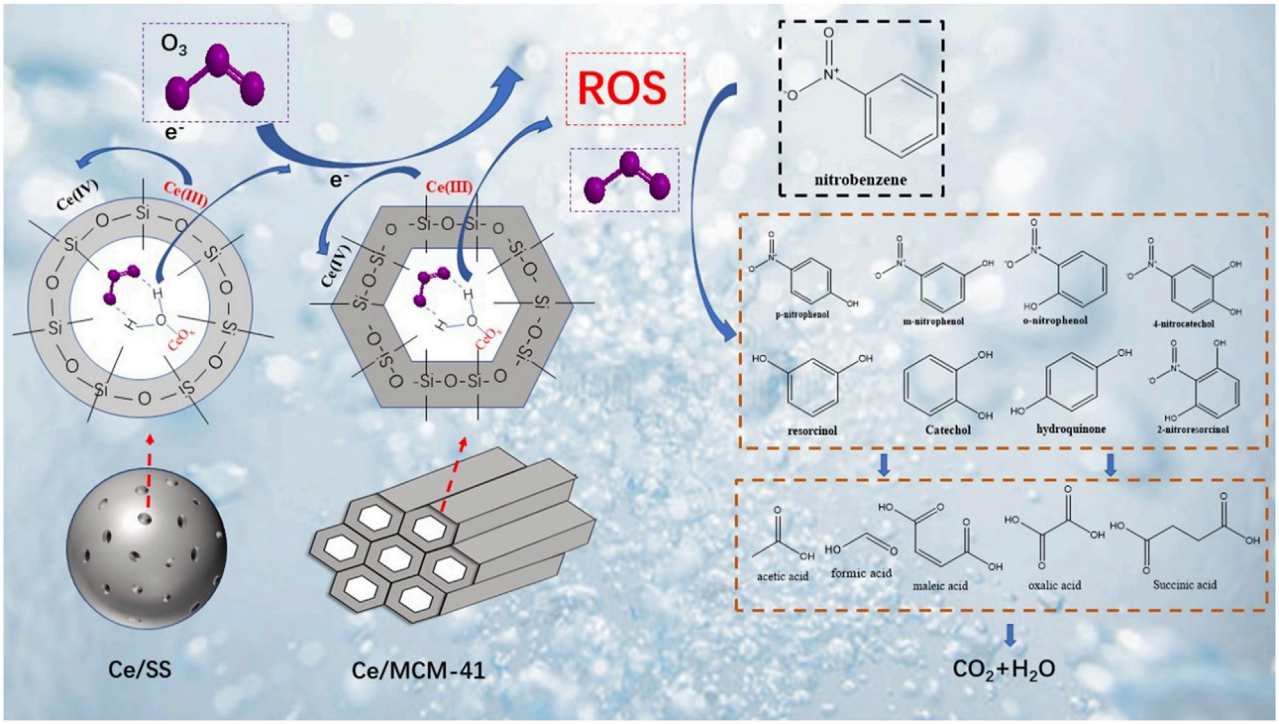

GRAPHICAL ABSTRACT

Introduction

The accompanying environment pollutions, especially the water pollutions, as the side-effects of the boosted development in civilization and industrialization of the human society have greatly threatened the health of human beings and the natural life (Tarpeh and Chen 2021). Refractory organic contaminants (ROCs) discharged from petrochemical wastewater such as phenolics and nitroaromatics obtain high ecotoxicity and are recalcitrant to be naturally degraded (Liu et al., 2021a). Additionally, most of degradation intermediates of these ROCs are even more toxic and possess intensive threats to the nature. It is of great significance to develop fast and complete mineralization techniques to treat these ROCs.

As a capable branch of advanced oxidation processes (AOPs), catalytic ozonation process (COP) offers a fast pollutants degradation rate and a high mineralization efficiency (Wang and Chen 2020; Liu et al., 2021b). With the presence of catalysts, the generated reactive oxygen species (ROS) such as hydroxyl radicals (·OH) and surface adsorbed oxygen atoms ($*O_{ad}$) by O_3 activation are responsible for rapid and complete treatment of ROCs owing to their high oxidation potentials (Yu et al., 2020; Jin et al., 2021). In recent studies, the prevailing carbonaceous catalysts such as activated carbon (Xiong et al., 2020), graphene-based nanocarbons (Wang et al., 2020; Zhang et al., 2021), and wasted carbon-derived catalysts (Chen et al., 2019) demonstrated outstanding catalytic ozonation activities for ROCs degradation. Nevertheless, high catalytic activities usually tied with unstable structures (Xiao et al., 2017; Li et al., 2021). During the reactions, carbon-based catalysts, especially those nanocarbons, are prone to be deactivated because of the variations of the surface chemistry and even the collapse of the carbon skeleton (Xiao et al., 2017). In addition, the singlet oxygenation and surface O_3 direction oxidation induced by the carbonaceous catalysts can efficiently oxidize the electron-rich ROCs, yet they obtain weak mineralization abilities (Xie et al., 2022).

Silica-based zeolites obtain robust structures and their rich surface Lewis acidic sites can be easily hydroxylated to form silanol structures, which accelerate the O_3 adsorption to produce ·OH (Valdés et al., 2012; Song et al., 2022). Furthermore, the rich channels with the zeolites and their high specific surface area facilitate the surface modification by active metal oxides (Li et al., 2020). Recent years, SBA-15 and MCM-41 loaded with transitional metal oxides such as MnO_2 and Co_3O_4 have been fruitfully synthesized as ozonation catalysts for efficient treatment of ROCs (Tang et al., 2017; Li et al., 2019; Zhang et al., 2020; Ma et al., 2022). However, the leaching of these active transitional metal oxides components can result in secondary pollution issues because of their high toxicity. Cerium oxide (CeO_2) is abundant in Earth and obtains much less toxicity than Co and Mn. Additionally, the special storage oxygen ability and

the electron transfer among the multivalence enable CeO_2 a proficient ozonation catalyst (Orge et al., 2012; Afzal et al., 2019).

In this work, CeO_2 supported on silica spherule (SS) and MCM-41 which have different space configuration were synthesized and employed as the ozonation catalysts for NB mineralization. Influence of solution pH on both adsorption capabilities and catalytic ozonation efficiencies were evaluated. In addition, to unveil the mechanistic insights into the Ce-doped silica catalysts for catalytic ozonation, multiscale characterizations such as the spectroscopy (XPS) and pyridinic Fourier transformed infrared spectroscopy (py-FTIR) were performed to investigate surface chemistry and the potential active sites. A combined quenching and *in situ* electro paramagnetic resonance (EPR) study was further conducted to probe the generated ROS and their roles in NB degradation. Additionally, the detailed NB degradation route was proposed based on the multi-chromatography analysis results.

Materials and methods

Chemicals

SS and MCM-41 were purchased from Shanghai Sunny Molecular Sieve Co., Shanghai, China. Sodium hydroxide (NaOH; AR), hydrochloric acid (HCl; AR), NB ($C_6H_5NO_2$; AR), Cerium (III) nitrate hexahydrate ($Ce(NO_3)_3{\cdot}6H_2O$; AR) were obtained from Beijing Chemical Reagents Co., China. Furfuryl alcohol (FFA; AR), tert-Butanol (TBA; AR) and p-benzoquinone (p-BQ) were purchased from Aladdin Reagent Co., Ltd., Shanghai, China. 5,5-Dimethyl-1-pyrroline (DMPO; GC grade) and 4-amino-2,2,6,6-tetramethylpiperidine (TEMP; GC grade) were procured from Sigma-Aldrich Inc. All the chemicals were used without further purification. The standard chemicals used to quantify the concentrations of degradation intermediates were listed in Supplementary Text S1 in Supporting Information.

Catalysts preparation

An incipient wetness impregnation method was employed to prepare the CeO_2 loaded SS and MCM-41 catalysts. In a typical synthesis, 48.8 g of SS or MCM-41 was saturated with a Ce^{3+} solution containing 1.56 g $Ce(NO_3)_3{\cdot}6H_2O$ and 35 ml of ultrapure water. The mixed sample was sonicated for 30 min and then kept 24 h at room temperature, which was followed by drying in an oven at 80 C for 6 h. The dried sample was then grounded and calcined in a muffle furnace in air at 550°C for 4 h. In accordance with the support used, the prepared sample was denoted as Ce/SS and Ce/MCM-41, respectively. The theoretical content of loaded CeO_2 for both catalysts was approximately 1 wt%.

Characterizations

Powder X-ray diffraction (XRD) was measured on an XRD-6000 powder diffraction instrument (Shimadzu, Kyoto, Japan) in the 2θ range of 0.5–90°, utilizing an accelerated voltage of 40 kV with Cu Kα radiation (λ = 1.5418 Å). The morphology of samples was examined on a Tecnai G2 F20 transmission electron microscope (TEM) (FEI, Hillsboro, OR, United States). The N_2 adsorption and desorption isotherms were obtained from an ASAP 2000 accelerated surface area and porosimetry system (Micromeritics, Norcross, GA, United States). The relative amounts of Lewis acid sites were measured by pyridine Fourier-transformed infrared spectroscopy (py-FTIR) on a Nicolet iS10 FT-IR spectrometer (Thermo Scientific, Waltham, MA, United States). Surface element distribution was recorded by a PHI Quantera SXM X-ray photoelectron spectrometer (XPS) (ULVAC-PHI, Chanhassen, MN, United States). Binding energy shift was calibrated by using C1s (B.E. = 284.8 eV) as the standard. The pH for point zero charge (pH_{pzc}) of the catalysts was determined according to the pH-drift method (Davranche et al., 2003). Electron spin resonance (ESR) experiments were performed on a Bruker EMX-Plus spectrometer to identify the types of reactive oxygen species (ROS). The microwave frequency was 9.057 GHz, the modulation frequency was 100 GHz and the microwave power was set as 10.00 mW.

Catalytic ozonation procedure

The COP experiments were performed according to the previous study (Chu et al., 2020). Gaseous ozone produced by the pure O_2 (99.999%) with the concentration of 7.5 mg min^{-1} was bubbled at the bottom of the reactor. In a typical test, 1 g L^{-1} of the catalyst was dosed into the NB solution (100 mg L^{-1}) and allowed to be stirred for 15 min to achieve sorption equilibrium. During the test, samples were withdrawn from the reactor at fixed time intervals and filtered by the 0.45 μm PTFE filter once O_3 was injected. A 7890B gas chromatographer integrated with a 5977B mass spectrometer (GC-MS, Agilent, Santa Clara, United States) was employed for identifying the intermediate products of NB. Concentrations of NB and its degradation intermediates were quantified by a high-performance liquid chromatography (HPLC, Thermo Scientific™ UltiMate™ 3,000, Waltham, United States). The detailed measurement methods were summarized in Supplementary Table S2. Additionally, a Dionex Aquion Ion Chromatograph (IC, Thermo Scientific, Waltham, United States) which equipped with an AG11-HC column (4 × 250 mm), was used to measure small molecular organic acids during the NB degradation. To determine the mineralization rate of NB, total organic carbon (TOC) was measured by a TOC-L CPH CN 200 TOC analyzer (Shimadzu, Kyoto, Japan). During the COP experiments, the

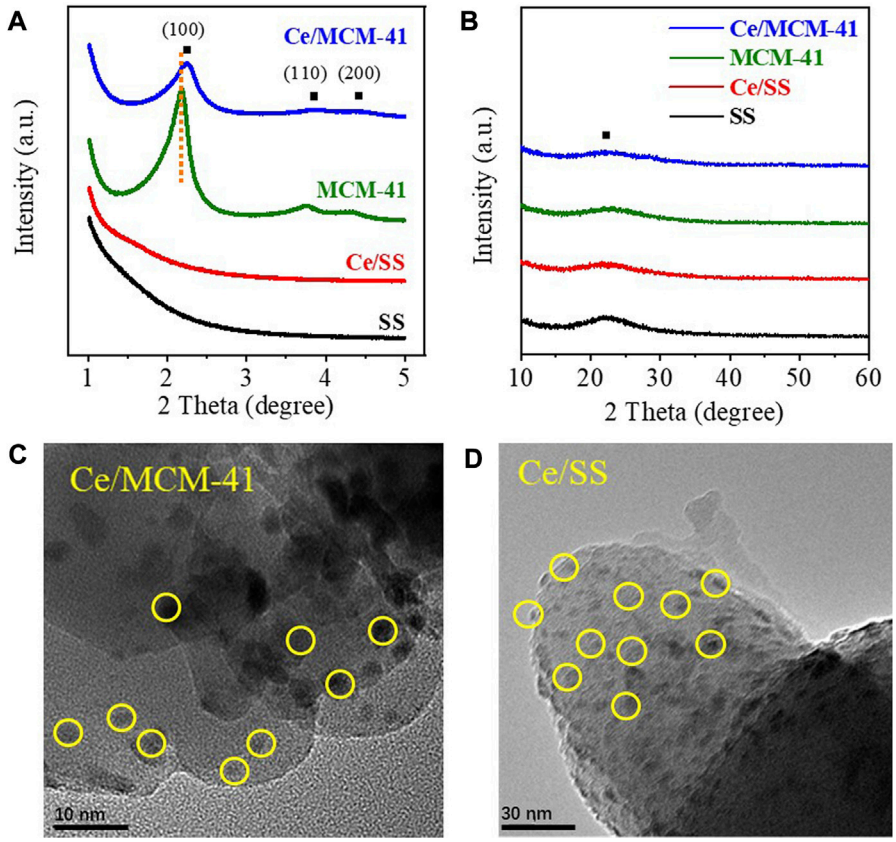

FIGURE 1
(A, B) XRD spectra of silica-based catalysts; **(C)** TEM image of Ce/MCM-41; **(D)** TEM image of Ce/SS.

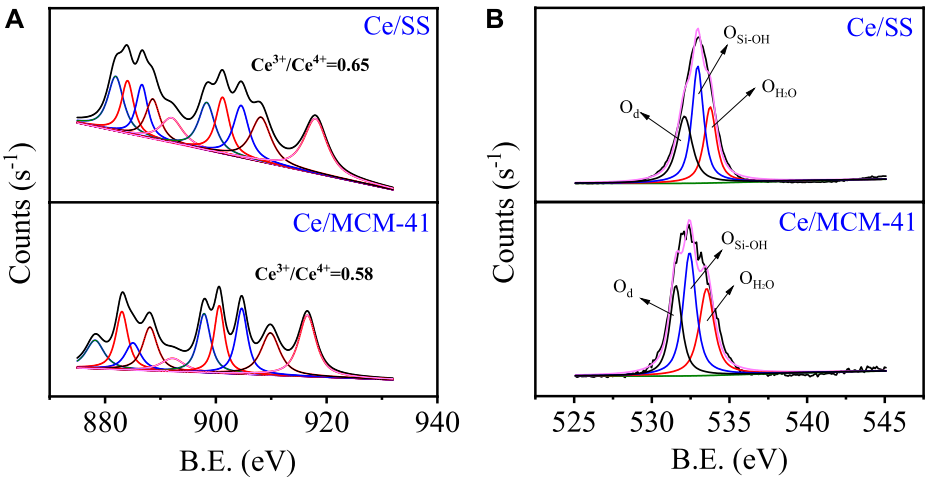

FIGURE 2
High resolution XPS spectra on Ce 3d **(A)** and O1s **(B)** for Ce/SS and Ce/MCM-41.

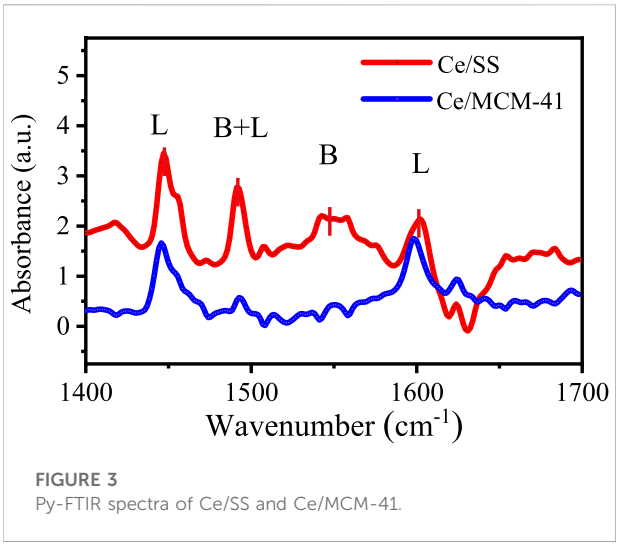

FIGURE 3
Py-FTIR spectra of Ce/SS and Ce/MCM-41.

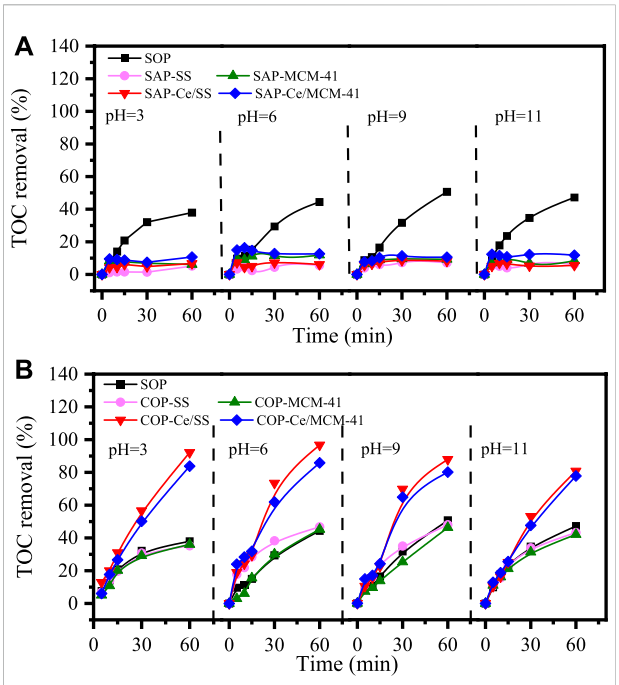

FIGURE 4
Comparison in TOC removal rates under different solution pHs for SAPs **(A)** and COPs **(B)** using as-synthesized catalysts. Reaction condition: Catalyst: 1 g L^{-1} catalyst; ozone concentration: 10 mg/min; temperature: 25°C $[NB]_0$=100 mg L^{-1}.

concentration of leached Ce was measured by an ICP-AES (Perkin Elmer DV7000, Waltham, MA, United States). All the catalytic ozonation tests were triplicate performed and the average values were provided.

Results and discussion

Characterization of the as-synthesized catalysts

Typical characteristic peaks centered at 2.2°, 3.8°, 4.4° were observed in the low-angle XRD pattern of MCM-41, which can be accordingly indexed to the (100), (110), and (200) facets of the ordered hexagonal structure (Figure 1A). The corresponding TEM observation in Supplementary Figure S1 also illustrated this ordered structure. On the contrary, no such diffraction peaks nor ordered lattice were discerned for SS and the existence of a broad diffraction peak centered at 2θ = 23° in the wide-angle XRD pattern (Figure 1B) was attributed to the amorphous SiO_2. Loading CeO_2 induced negligible changes to the XRD patterns of MCM-41 and SS, which can be ascribed to the low loading amount and high dispersion of CeO_2. For Ce/MCM-41, the low-angle XRD pattern revealed that the diffraction peak for (100) facet was shifted to a higher diffraction angle compared to that of MCM-41, suggesting the loading of CeO_2 increased the interplane spacing of the original lattice structure of MCM-41. TEM images further displayed the successful loading of CeO_2 on the MCM-41 and SS (Figures 1C,D). For both Ce/MCM-41 and Ce/SS, CeO_2 were evenly dispersed on the surface of MCM-41 and SS. Specific surface areas (SSAs) and the pore information of the materials were derived from the N_2-sorption isotherms and the corresponding pore size distributions, respectively (Supplementary Figure S2). Compared to SS, MCM-41 possesses greater SSA (1,024 vs. 491 m^2/g) and pore volume (0.93 vs. 0.75 cm^3/g). Both the SSA and pore volume of Ce/MCM-41 and Ce/SS decreased after loading CeO_2 (Supplementary Table S1), because the formed CeO_2 clusters occupied the surface or blocked the partial pore of the substrates.

XPS was employed to investigate the surface chemistry of Ce/MCM-41 and Ce/SS (Figure 2). The high-resolution Ce 3d surveys of the samples could be deconvoluted into Ce 3d5/2 and Ce 3d3/2 spin–orbit split doublets, which were further fitted with ten peaks (Anandan and Bera 2013). The peaks at 881.9, 886.7, 898.3, and 904.5 eV represent Ce^{3+} and the peaks at 884.1, 888.5, 891.8, 901.3, 907.9, and 917.8 eV were identified as Ce^{4+}. Based on the deconvolution results, the Ce^{3+}/Ce^{4+} ratios could be derived by the corresponding integral peak areas and are listed in Supplementary Table S1. Evidently, Ce/SS obtained a higher Ce^{3+}/Ce^{4+} ratio than that of Ce/MCM-41 (0.65 vs. 0.31), indicating that SS has a more reductive surface than that of MCM-41. Additionally, the higher composition of Ce^{3+} in Ce/SS than that of Ce/MCM-41 might be ascribed to the existence of higher amount of oxygen vacancies. The high-resolution O 1s XPS surveys of the Ce/SiO_2 catalysts were further deconvoluted to evaluate the composition of the surface oxygen species. The peaks at 532.0, 532.8, and 533.5 eV can be indexed to the lattice oxygen (O_{lat}), surface hydroxyl groups/oxygen vacancy (O_{-OH}/

O_v), and surface adsorbed H_2O species (O_{H2O}), respectively. A greater proportion of O_{-OH}/O_v was identified on Ce/SS than that of Ce/MCM-41 (0.58 vs. 0.37). Previous studies suggested that the both O_{-OH} and O_v can function as the Lewis acidic sites, which facilitated the O_3 adsorption and the subsequent dissociation into ROS (Yu et al., 2020).

Py-FTIR measurements were further performed to investigate the types of the acidic sites and Lewis acidity of the Ce/SiO_2 catalysts (Figure 3). IR bands centered around 1,446 cm^{-1} and 1,598 cm^{-1} were discerned, which could be ascribed to pyridine adsorbed on Lewis acids sites. The peaks centered at 1,544 and 1,491 cm^{-1} were assigned to the pyridine adsorbed on strong Brønsted acid and both Lewis and Brønsted acid sites, respectively (Xu et al., 2019). For both catalysts, the intensities of Lewis acid peaks were notably higher than those of Brønsted acid, suggesting Lewis acid was the main acid sites. Meanwhile, Lewis acid peak intensities of Ce/SS were significantly greater than those of Ce/MCM-41, revealing the presence of higher amount of Lewis acidic sites on Ce/SS than that of Ce/MCM-41. The higher amount of Lewis acidic sites also led to the greater reducibility, which agreed well with the XPS analysis results.

Catalytic efficiencies and active sites

Prior to evaluating the catalytic ozonation performance of the catalysts, single adsorption tests (SAP) and single ozonation treatment (SOP) were performed as the benchmarks. Adsorption by Ce/MCM-41 and Ce/SS resulted in 11.9 and 5.5% TOC removal within 60 min at pH 6, revealing the minor contribution of adsorption to NB removal (Figure 4A). Additionally, decrease or increase of solution pH resulted in trivial variations in adsorption capabilities. With the pKa value of 11.9, NB existed in its molecular form. The pH point of zero charges (pH_{pzc}s) of Ce/MCM-41 and Ce/SS were determined as 3.2 and 5.4, respectively. Therefore, the negligible electrostatic interaction between the neutrally charged NB and the negatively charged catalysts induced marginal electrostatic adsorption. And the higher adsorption capacity of Ce/MCM-41 than that of Ce/SS can be ascribed to its larger SSA. Meanwhile, the greater pH_{pzc} value of Ce/SS than that of Ce/MCM-41 agreed with the py-FTIR results because the zeta potential would be enhanced by the increased amount of surface Lewis acidic sites. In the SOP test, around 45% TOC mineralization was achieved at pH 6, suggesting the inability of single ozonation treatment for NB destruction.

For catalytic ozonation processes (COPs), trivial TOC mineralization enhancements were observed with the presence of MCM-41 and SS compared to that of SOP, indicating the SiO_2 substrates obtained marginal catalytic ozonation activities (Figure 4B). Contrarily, substantial augments in TOC mineralization rates were discerned by utilizing Ce modified SiO_2 as the catalysts. With the solution pH 6, 86 and 97% TOC mineralization was achieved for Ce/MCM-41 and Ce/SS accordingly, confirming the crucial role of CeO_2 on silica-based materials in boosting the catalytic ozonation activities. Ce^{3+} leaching was also tested by ICP-AES for catalytic ozonation over Ce/SS and Ce/MCM-41 and around 0.3 mg/L of Ce^{3+} was detected for both catalytic ozonation systems. Considering the low catalytic ozonation activity of Ce^{3+} (Orge et al., 2012), this trace amount of Ce^{3+} contributed trivially to NB mineralization in form of homogeneous catalysis.

To determine the real catalytic performance of the as-synthesized materials, TOC mineralization rates by COPs were subtracted by the corresponding TOC removal rates of SAPs and SOPs. As the result, a 46 and 29% increase in TOC mineralization rate was achieved for Ce/SS and Ce/MCM-41 at pH 6, respectively. Though the SSA of Ce/MCM-41 was 2.1-fold higher than that of Ce/SS (1,024 vs. 491 m^2/g), Ce/MCM-41 demonstrated an inferior catalytic activity than Ce/SS. The significant improvement in catalytic activity for Ce/SS can be ascribed to the elevated amount of surface Lewis acidic sites, which are well illustrated through the characterizations. Apart from the intrinsic surface hydroxyl groups, the oxygen vacancies also facilitate the adsorption of ambient water molecules, which subsequently transform into hydroxyl groups via surface hydroxylation process (Yu et al., 2020). Both intrinsic and extrinsic hydroxyl groups can induce the interaction between the O_3 molecules and their dissociation into ROS. On the other hand, oxygen vacancy sites also favored the chemisorption of O_3 molecules and their subsequent evolution into ROS. Additionally, the high reducibility of SS surface created greater amount of Ce^{3+} than that of MCM-41. The Ce^{3+}/Ce^{4+} redox cycle further boosted the electron transfer between the O_3 and the Lewis acidic sites and promoted the catalytic activity.

Influence of initial pH on ozonation activities was also evaluated. For single ozonation treatment, increasing the initial pH from three to nine enhanced the TOC removal rate (37.9 ~ 50.7%), while further increasing the initial solution pH to 11 slightly inhibited the TOC abatement rate (47.2%). It is suggested that OH^- could promote ozone decomposition to generate ·OH, thus TOC removal could be enhanced in ozonation systems with higher pH values (Zhu et al., 2017). However, the over abundant OH^- might deplete the produced ·OH and thus suppressed the TOC removal rate (Cheng et al., 2020). Both Ce/SS- and Ce/MCM-41-driven catalytic ozonation systems demonstrated good treatment compatibility to a wide pH range and Ce/SS obtained a greater TOC removal efficiency than Ce/MCM-41. Noted that, TOC mineralization rates reached maximum when initial solution pH values were close to pH_{pzc} values of Ce/SS and Ce/MCM-41 (3.2 and 5.4). A 47.6 and 35.2% improvement in TOC mineralization was achieved for Ce/SS/O_3 and Ce/MCM-41/O_3 at pH three and pH six accordingly, compared to their single ozonation treatments. It is suggested that the relaxation of the electric double layer (EDL) on surface of

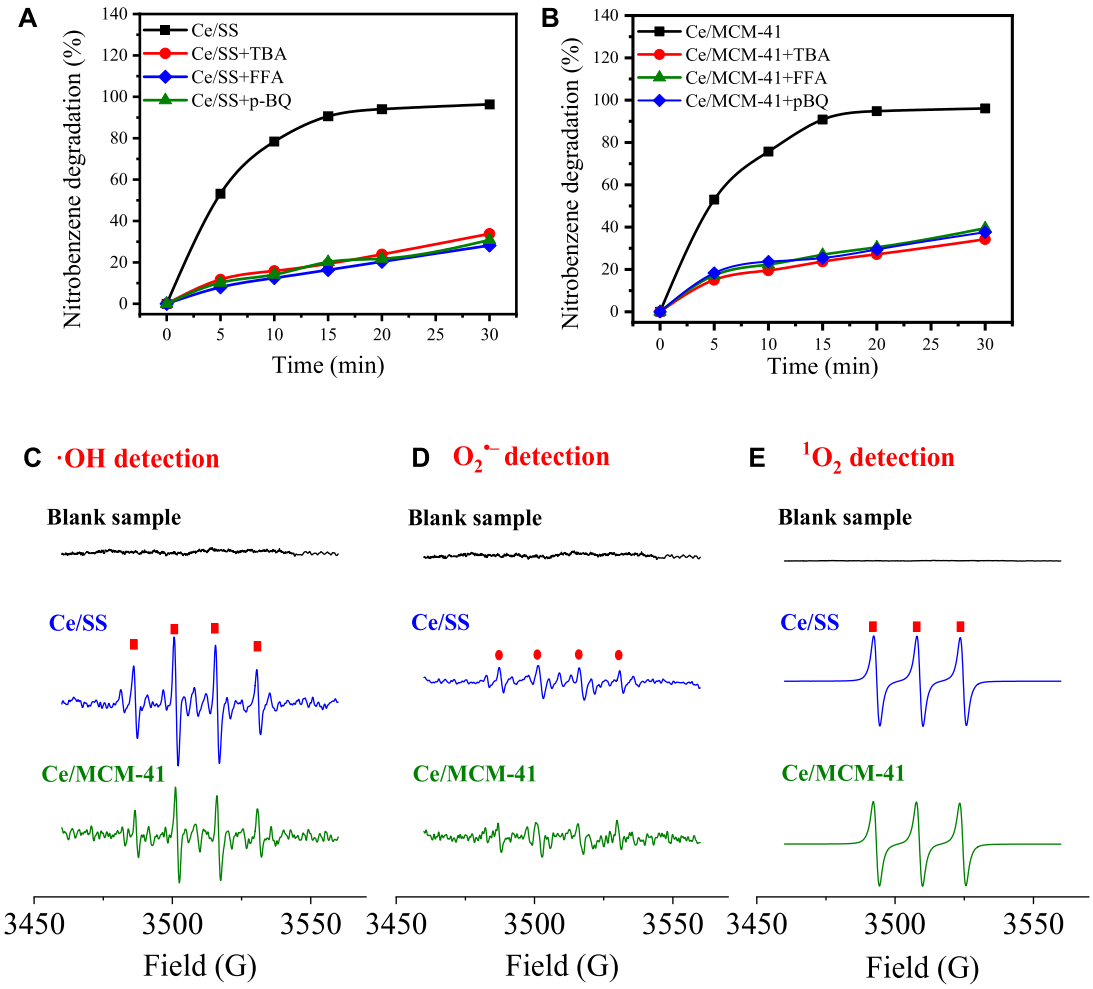

FIGURE 5
Radical quenching tests for catalytic ozonation using Ce/SS **(A)** and Ce/MCM-41 **(B)**; *In situ* EPR spectra for ·OH **(C)**, $O_2^{\bullet-}$ **(D)**, and $1O_2$ **(E)** identification in Ce/SS- and Ce/MCM-41- driven COPs.

the catalysts facilitated the inner-sphere interaction with O_3 molecules and their subsequent evolution into ·OH (Wang et al., 2020). When initial pH values are higher than the pH_{pzc}, the deprotonated surface as well as the compressed EDL inhibited the chemisorption of O_3. For pH < pH_{pzc} of the catalysts, although the protonated surface could act as the Lewis acidic sites promoting the attraction of the O_3 molecules, the slightly compression of the EDL hindered this process.

Generated ROS and the possible reaction mechanisms

Quenching tests were carried out to investigate the possible generated ROS for NB degradation (Figures 5A,B). The as-mentioned strong inner-sphere interaction between the surface Lewis acidic sites and O_3 molecules is prone to induce the formation of ·OH, which has been recognized as the prevailing ROS produced in metal-based catalysts-driven catalytic ozonation processes (Liu et al., 2021b; Liu et al., 2022). To investigate the contribution of ·OH in NB degradation, TBA which obtains low react rate with O_3 (k_{O_3}=3 × 10^{-5} M^{-1} s^{-1}) but can rapidly react with ·OH ($k_{\cdot OH}$= 3.8 × 10^8–7.6×10^8 $M^{-1}s^{-1}$) was employed as the quenching agent (Wang et al., 2022). Addition of 15 mM of TBA to both Ce/SS/O_3 and Ce/MCM-41/O_3 systems significantly inhibited 62% of the NB degradation, revealing the dominant role of ·OH in NB degradation. To semi-quantify the ·OH produced amounts in these catalytic ozonation systems, *in situ* EPR measurements were performed. To better trap the produced ROS, the withdrawn samples were immediately mixed with DMPO solution and cryo-frozen by liquid nitrogen. Figure 5C

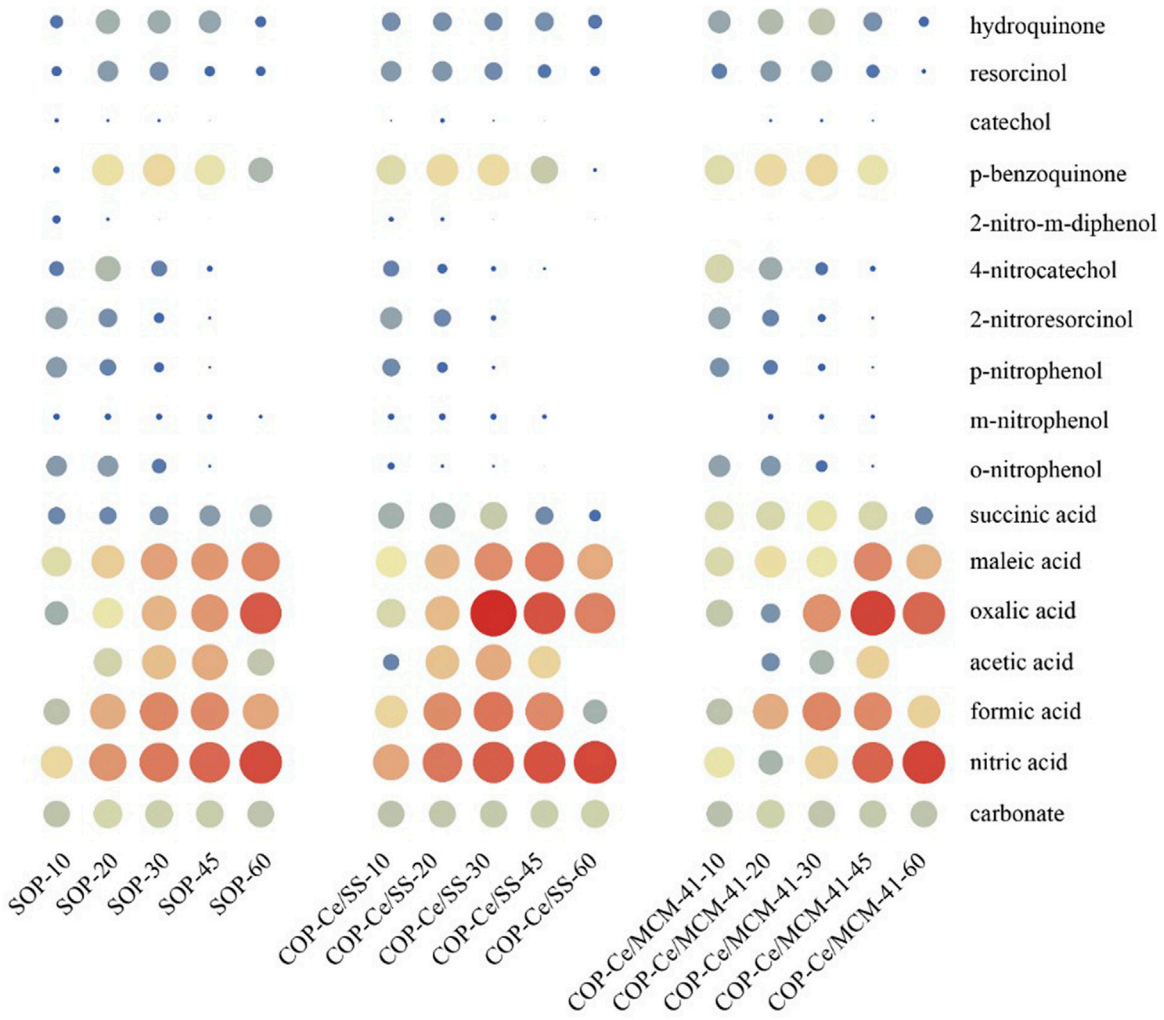

FIGURE 6
Heatmap diagrams of intermediate products of NB degradation in COPs with the Ce/Si catalysts.

displays that the intensity of DMPO-·OH adduct in Ce/SS/O_3 is greater than that in Ce/MCM-41/O_3, suggesting a higher amount of ·OH was produced, which explained the higher TOC removal rate. DMPO-·OOH adducts with the hyperfine couplings of a_N=14.2 G, a_H^{β}=11.4 G, a_H^{γ}=1.2 G were identified by addition methanol to the DMPO solution (Figure 5D), suggesting the existence of superoxide radicals ($O_2^{\bullet-}$) (Wang et al., 2020). However, $O_2^{\bullet-}$ obtained a less oxidation potential than ·OH (1.7 vs. 2.7 V), making it fail to oxidize the recalcitrant organics such as NB. The corresponding quenching test with the addition of pBQ (0.5 mM), which is an effective scavenger for both $O_2^{\bullet-}$ ($k_{HO_2^-/O_2^-}$= 3.5 × 10^8–7.8×10^8 $M^{-1}s^{-1}$) and ·OH ($k_{\cdot OH}$= 1.2×10^9 $M^{-1}s^{-1}$) (Samoilova et al., 2011), resulted in a similar inhibition degree to that of TBA. Therefore, $O_2^{\bullet-}$ was the pivotal intermediate for ·OH formation in this process. Apart from ·OH and $O_2^{\bullet-}$, the characteristic EPR signal for singlet oxygen ($^1O_2$) was also identified by using TEMP as the spin trapping agent (Figure 5E). Notably, trace amount of pBQ was added to the TEMP solution to quench the produced ·OH and $O_2^{\bullet-}$, which can also oxidize TEMP to form the triplet TEMPO EPR signals. TEMP solution pH was also adjusted to three to avoid the alkaline activation of O_3. Although $^1O_2$ was generated, its low oxidation potential (0.85 V) hindered the attack to the recalcitrant NB. The overlapped NB degradation curves for TBA and FFA quenching tests further confirm the incapability of $^1O_2$ to degrade NB. The combined results of quenching tests and the *in situ* EPR measurements revealed that ·OH was the predominated ROS for NB degradation and the mineralization. $O_2^{\bullet-}$ and $^1O_2$ contributed marginally to NB degradation, yet they can oxidize the less-recalcitrant intermediates and facilitate their degradation. The following equations (Eqs. (1)-(7)) are the possible routes for generation and evolution of these ROS on

the Lewis acidic sites of Ce/SiO_2 catalysts, where -Me^{n+}, V_o, and $O_o^{\times}$ denote the Lewis acidic sites metal cations, the doubly charged OV, and the oxygen ion in a normal oxygen site, respectively.

$$-Me^{n+} + H_2O \rightarrow -Me^{n+} - OH + H^+ \quad (1)$$

$$-Me^{n+} - OH + O_3 \rightarrow -Me^{n+} - O_3^{\bullet} + {\bullet}OH \quad (2)$$

$$-Me^{n+} - O_3^{\bullet} + OH^- \rightarrow -Me^{n+} + HO_2^{\bullet} + O_2 \quad (3)$$

$$V_o + O_3 + H_2O \rightarrow O_o^{\times} + OH + H^+ + O_2 \quad (4)$$

$$HO_2^{\bullet} \rightarrow H^+ + O_2^{\bullet -} \quad (5)$$

$$O_2^{\bullet -} + {\bullet}OH \rightarrow {}^1O_2 + OH^- \quad (6)$$

$$HO_2^{\bullet} + O_2^{\bullet -} \rightarrow {}^1O_2 + HOO^- \quad (7)$$

Evaluation of NB degradation intermediate and degradation pathways

A combined analysis of GC-MS, HPLC and IC was employed to investigate the degradation intermediates and their concentrations. The identified degradation intermediates and their detection techniques were summarized in Supplementary Table S3. The heatmap diagrams derived from the quantitative analysis of intermediate products from different oxidation systems were shown in Figure 6. Polyhydroxy phenols, p-BQ and small molecular aliphatic acids were the main intermediates in catalytic ozonation systems. Compared to the SOP, COPs possessed much faster NB oxidation to form benzoquinone. Furthermore, the formed benzoquinone could be mineralized more rapidly than SOP. The formed aliphatic acids such as oxalic acid, formic acid and maleic acid as the terminal intermediates gradually accumulated and can hardly be oxidized in single ozonation treatment. In contrast, the accumulated aliphatic acids would be destructed in catalytic ozonation processes. The variations of solution pH during the oxidation processes further confirmed the production of these aliphatic acids followed by their mineralization (Supplementary Figure S3).

Based on the identified degradation intermediates and their evolution trends, the proposed pathways for NB degradation in catalytic ozonation with CeO_2/SiO_2 catalysts were thus deduced (Supplementary Figure S4). It was assumed that electron transfer, electrophilic addition, and nucleophilic substitution reaction can participate in the degradation of NB via the following three stages (Zhao et al., 2008): 1) Phenyl radicals and nitrophenyl radicals were formed by electron transfer process between the ROS and NB molecules. Then phenyl radicals and nitrophenyl radicals were oxidized to form polyhydroxyphenols by electrophilic addition (Li et al., 2006). 2) Denitration of NB could be attributed to the nucleophilic substitution reaction with ROS, and then polyhydroxyphenols were formed via electrophilic addition, which were further oxidized to benzoquinone (Wang et al., 2016; Yang et al., 2018). 3) Polyhydroxyphenols and benzoquinone would be further oxidized to form small molecular aliphatic acids such as formic acid, acetic acid, and oxalic acid as the terminal intermediates. These aliphatic acids were finally mineralized to CO_2 and H_2O by ·OH.

Reusability of catalysts in COP

Reusability of the as-synthesized Ce/SS and Ce/MCM-41 was evaluated by an 8-cycle stability test (Supplementary Figure S5). After each run, the used catalyst was collected by filtration and dried. The lost amount of the catalyst (approximately 5% in average) was compensated by addition of the fresh catalyst prior to the next use. After each run, concentration of the leached Ce^{3+} was examined by ICP-AES (Supplementary Table S2). Passivation was observed on both catalysts. TOC removal rate for Ce/SS reduced from 96.8 to 63.1% after eight reuses and TOC removal rate decreased from 92.8 to 47.1% using Ce/MCM-41. It was found that the accumulated Ce^{3+} leaching amount for the eight cycles of Ce/MCM-41 was almost twice as much as that of Ce/SS (1.3 vs. 2.5 mg/L). This result suggests the critical role of the Ce-O-Si bond in formation of surface Lewis acidic sites which facilitated the chemisorption of O_3 and the subsequent ROS formation.

Based on the limited leaching of Ce^{3+}, it could be deduced that the main reason for Ce/SiO_2 deactivation is the reduction of catalytic active sites with the surface covered by intermediates. Thus, mild annealing in the air (e.g., calcinated at 350°C for 3 h) is a feasible method for catalysts regeneration. On one hand, intermediates attached to the surface could be removed to expose catalytic active sites in the process of calcination. On the other hand, the carbon adsorbed on Ce/SiO_2 surface could also reduce the oxidized catalyst, which would further facilitate the recovery of activity.

Conclusion

Ce loaded silica catalysts were synthesized via a facile impregnation method and employed for catalytic ozonation of NB. Compared with pure SS and MCM-41, Ce/SS and Ce/MCM-41 with Ce loading dramatically increased the catalytic activities, resulting in the increment of the corresponding TOC mineralization rates by 46.2 and 35.8%, respectively. Based on the XPS analysis and py-FTIR results, higher amount of surface Lewis acidic sites were formed on silica catalysts with Ce loading than the pure silicas, which accounted for the activity enhancement. The Ce^{3+}/Ce^{4+} redox cycle further accelerated the electron transfer. Additionally, influence of solution pH on catalytic activities was also investigated. It was

found that the catalysts obtained the highest activities when pH was closed to their pH_{pzc}s, confirming the critical roles of Lewis acidic sites in catalytic performance. Results from radical quenching tests suggested that although ·OH, $O_2^{\bullet-}$ and $^1O_2$ were produced during the catalytic ozonation process, ·OH is the dominant ROS for NB mineralization. Chromatography analysis suggested that NB was firstly oxidized into polyhydroxy compounds, followed by small molecular organic acids and finally being mineralized into CO_2 and H_2O. This study demonstrated the potential and mechanisms of the Ce/SiO_2 catalysts in COP treatment of recalcitrant chemical wastewaters.

Data availability statement

The raw data supporting the conclusions of this article will be made available by the authors, without undue reservation.

Author contributions

QW: Sample preparation, experimental design and writing; YJ: sample preparation, investigation and original draft; HY: Data interpretation and investigation; JH: Data interpretation and investigation; YL: Data interpretation and reviewing; YW: Conceptualization, writing, reviewing and editing; CC: Conceptualization, reviewing and editing; ZL: reviewing and editing.

Funding

This study was supported in part by the National Natural Science Foundation of China (No. 21776307, 21978324 and 22278436) and Science Foundation of China University of Petroleum, Beijing (No. 2462020YXZZ034, 2462022XKBH002 and 01JB20220078).

Conflict of interest

The authors declare that the research was conducted in the absence of any commercial or financial relationships that could be construed as a potential conflict of interest.

Publisher's note

All claims expressed in this article are solely those of the authors and do not necessarily represent those of their affiliated organizations, or those of the publisher, the editors and the reviewers. Any product that may be evaluated in this article, or claim that may be made by its manufacturer, is not guaranteed or endorsed by the publisher.

Supplementary material

The Supplementary Material for this article can be found online at: https://www.frontiersin.org/articles/10.3389/fenvs.2022.1040276/full#supplementary-material

References

Afzal, S., Quan, X., and Lu, S. (2019). Catalytic performance and an insight into the mechanism of CeO_2 nanocrystals with different exposed facets in catalytic ozonation of p-nitrophenol. *Appl. Catal. B Environ.* 248, 526–537. doi:10.1016/j.apcatb.2019.02.010

Anandan, C., and Bera, P. (2013). XPS studies on the interaction of CeO_2 with silicon in magnetron sputtered CeO_2 thin films on Si and Si_3N_4 substrates. *Appl. Surf. Sci.* 283, 297–303. doi:10.1016/j.apsusc.2013.06.104

Chen, C., Yan, X., Xu, Y., Yoza, B. A., Wang, X., Kou, Y., et al. (2019). Activated petroleum waste sludge biochar for efficient catalytic ozonation of refinery wastewater. *Sci. Total Environ.* 651, 2631–2640. doi:10.1016/j.scitotenv.2018.10.131

Cheng, J., Wang, D., Wang, B., Ning, H., Zhang, Y., Li, Y., et al. (2020). Plasma-catalytic degradation of ciprofloxacin in aqueous solution over different MnO_2 nanocrystals in a dielectric barrier discharge system. *Chemosphere* 253, 126595. doi:10.1016/j.chemosphere.2020.126595

Chu, L., Sun, Z., Cang, L., Fang, G., Wang, X., Zhou, D., et al. (2020). A novel sulfite coupling electro-fenton reactions with ferrous sulfide cathode for anthracene degradation. *Chem. Eng. J.* 400, 125945. doi:10.1016/j.cej.2020.125945

Davranche, M., Lacour, S., Bordas, F., and Bollinger, J.-C. (2003). An easy determination of the surface chemical properties of simple and natural solids. *J. Chem. Educ.* 80 (1), 76. doi:10.1021/ed080p76

Jin, X., Wu, C., Tian, X., Wang, P., Zhou, Y., and Zuo, J. (2021). A magnetic-void-porous $MnFe_2O_4$/carbon microspheres nano-catalyst for catalytic ozonation: Preparation, performance and mechanism. *Environ. Sci. Ecotechnol.* 7, 100110. doi:10.1016/j.ese.2021.100110

Li, Q., Gu, C., Di, Y., Yin, H., and Zhang, J. (2006). Photodegradation of nitrobenzene using 172 nm excimer UV lamp. *J. Hazard. Mat.* 133 (1), 68–74. doi:10.1016/j.jhazmat.2005.09.061

Li, S., Li, X., Wu, H., Sun, X., Gu, F., Zhang, L., et al. (2019). Mechanism of synergistic effect on electron transfer over Co–Ce/MCM-48 during ozonation of pharmaceuticals in water. *ACS Appl. Mat. Interfaces* 11 (27), 23957–23971. doi:10.1021/acsami.9b02143

Li, S., Wang, J., Ye, Y., Tang, Y., Li, X., Gu, F., et al. (2020). Composite Si-O-metal network catalysts with uneven electron distribution: Enhanced activity and electron transfer for catalytic ozonation of carbamazepine. *Appl. Catal. B Environ.* 263, 118311. doi:10.1016/j.apcatb.2019.118311

Li, M., Liu, D., Chen, X., Yin, Z., Shen, H., Aiello, A., et al. (2021). Radical-driven decomposition of graphitic carbon nitride nanosheets: Light exposure matters. *Environ. Sci. Technol.* 55 (18), 12414–12423. doi:10.1021/acs.est.1c03804

Liu, J., Ye, R., Shi, J., Wang, H., Wang, L., Jian, P., et al. (2021a). Construction of Cu nanoparticles embedded nitrogen–doped carbon derived from biomass for highly boosting the nitrobenzene reduction: An experimental and theoretical understanding. *Chem. Eng. J.* 419, 129640. doi:10.1016/j.cej.2021.129640

Liu, Y., Chen, C., Duan, X., Wang, S., and Wang, Y. (2021b). Carbocatalytic ozonation toward advanced water purification. *J. Mat. Chem. A* 9 (35), 18994–19024. doi:10.1039/d1ta02953c

Liu, B., Zhang, M., Yang, J., and Zhu, M. (2022). Efficient ozone decomposition over bifunctional Co_3Mn-layered double hydroxide with strong electronic interaction. *Chin. Chem. Lett.* 33 (10), 4679–4682. doi:10.1016/j.cclet.2022.01.025

Ma, D., Liu, W., Huang, Y., Xia, D., Lian, Q., and He, C. (2022). Enhanced catalytic ozonation for eliminating CH_3SH via stable and circular electronic

metal–support interactions of Si–O–Mn bonds with low Mn loading. *Environ. Sci. Technol.* 56 (6), 3678–3688. doi:10.1021/acs.est.1c07065

Orge, C. A., Órfão, J. J. M., Pereira, M. F. R., Duarte de Farias, A. M., and Fraga, M. A. (2012). Ceria and cerium-based mixed oxides as ozonation catalysts. *Chem. Eng. J.* 200-202, 499–505. doi:10.1016/j.cej.2012.06.088

Samoilova, R. I., Crofts, A. R., and Dikanov, S. A. (2011). Reaction of superoxide radical with quinone molecules. *J. Phys. Chem. A* 115 (42), 11589–11593. doi:10.1021/jp204891n

Song, J., Ma, N., Chen, W., Chen, J., and Dai, Q. (2022). Insights into mechanism of catalytic ozonation of cinnamyl alcohol over core–shell Fe_3O_4@SiO_2@La_2O_3 catalyst. *Sep. Purif. Technol.* 282, 119969. doi:10.1016/j.seppur.2021.119969

Tang, Y., Pan, Z., and Li, L. (2017). pH-insusceptible cobalt-manganese immobilizing mesoporous siliceous MCM-41 catalyst for ozonation of dimethyl phthalate. *J. Colloid Interface Sci.* 508, 196–202. doi:10.1016/j.jcis.2017.08.017

Tarpeh, W. A., and Chen, X. (2021). Making wastewater obsolete: Selective separations to enable circular water treatment. *Environ. Sci. Ecotechnol.* 5, 100078. doi:10.1016/j.ese.2021.100078

Valdés, H., Tardón, R. F., and Zaror, C. A. (2012). Role of surface hydroxyl groups of acid-treated natural zeolite on the heterogeneous catalytic ozonation of methylene blue contaminated waters. *Chem. Eng. J.* 211-212, 388–395. doi:10.1016/j.cej.2012.09.069

Wang, J., and Chen, H. (2020). Catalytic ozonation for water and wastewater treatment: Recent advances and perspective. *Sci. Total Environ.* 704, 135249. doi:10.1016/j.scitotenv.2019.135249

Wang, Y., Xie, Y., Sun, H., Xiao, J., Cao, H., and Wang, S. (2016). Efficient catalytic ozonation over reduced graphene oxide for p-hydroxylbenzoic acid (PHBA) destruction: Active site and mechanism. *ACS Appl. Mat. Interfaces* 8 (15), 9710–9720. doi:10.1021/acsami.6b01175

Wang, Y., Duan, X., Xie, Y., Sun, H., and Wang, S. (2020). Nanocarbon-based catalytic ozonation for aqueous oxidation: Engineering defects for active sites and tunable reaction pathways. *ACS Catal.* 10 (22), 13383–13414. doi:10.1021/acscatal.0c04232

Wang, Y., Li, X., Liu, S., Liu, Y., Kong, T., Zhang, H., et al. (2022). Roles of catalyst structure and gas surface reaction in the generation of hydroxyl radicals for photocatalytic oxidation. *ACS Catal.* 12, 2770–2780. doi:10.1021/acscatal.1c05447

Xiao, J., Han, Q., Xie, Y., Yang, J., Su, Q., Chen, Y., et al. (2017). Is C_3N_4 chemically stable toward reactive oxygen species in sunlight-driven water treatment? *Environ. Sci. Technol.* 51 (22), 13380–13387. doi:10.1021/acs.est.7b04215

Xie, Y., Liu, Y., Yao, Y., Shi, Y., Zhao, B., and Wang, Y. (2022). *In-situ* synthesis of N, S co-doped hollow carbon microspheres for efficient catalytic oxidation of organic contaminants. *Chin. Chem. Lett.* 33 (3), 1298–1302. doi:10.1016/j.cclet.2021.07.055

Xiong, W., Cui, W., Li, R., Feng, C., Liu, Y., Ma, N., et al. (2020). Mineralization of phenol by ozone combined with activated carbon: Performance and mechanism under different pH levels. *Environ. Sci. Ecotechnol.* 1, 100005. doi:10.1016/j.ese.2019.100005

Xu, Y., Lin, Z., Zheng, Y., Dacquin, J.-P., Royer, S., and Zhang, H. (2019). Mechanism and kinetics of catalytic ozonation for elimination of organic compounds with spinel-type $CuAl_2O_4$ and its precursor. *Sci. Total Environ.* 651, 2585–2596. doi:10.1016/j.scitotenv.2018.10.005

Yang, P., Luo, S., Liu, Y., and Jiao, W. (2018). Degradation of nitrobenzene wastewater in an acidic environment by Ti(IV)/H_2O_2/O_3 in a rotating packed bed. *Environ. Sci. Pollut. Res.* 25 (25), 25060–25070. doi:10.1007/s11356-018-2551-8

Yu, G., Wang, Y., Cao, H., Zhao, H., and Xie, Y. (2020). Reactive oxygen species and catalytic active sites in heterogeneous catalytic ozonation for water purification. *Environ. Sci. Technol.* 54 (10), 5931–5946. doi:10.1021/acs.est.0c00575

Zhang, J., Zhuang, T., Liu, S., Zhang, G. C., and Huo, K. (2020). Catalytic ozonation of phenol enhanced by mesoporous MnO_2 prepared through nanocasting method with SBA-15 as template. *J. Environ. Chem. Eng.* 8 (4), 103967. doi:10.1016/j.jece.2020.103967

Zhang, J., Xin, B., Shan, C., Zhang, W., Dionysiou, D. D., and Pan, B. (2021). Roles of oxygen-containing functional groups of O-doped g-C_3N_4 in catalytic ozonation: Quantitative relationship and first-principles investigation. *Appl. Catal. B Environ.* 292, 120155. doi:10.1016/j.apcatb.2021.120155

Zhao, L., Ma, J., and Sun, Z. (2008). Oxidation products and pathway of ceramic honeycomb-catalyzed ozonation for the degradation of nitrobenzene in aqueous solution. *Appl. Catal. B Environ.* 79 (3), 244–253. doi:10.1016/j.apcatb.2007.10.026

Zhu, H., Ma, W., Han, H., Han, Y., and Ma, W. (2017). Catalytic ozonation of quinoline using nano-MgO: Efficacy, pathways, mechanisms and its application to real biologically pretreated coal gasification wastewater. *Chem. Eng. J.* 327, 91–99. doi:10.1016/j.cej.2017.06.025